ATR2Cala2 from Arabidopsis-infecting downy mildew requires 4 TIR-NLR immune receptors for full recognition

New Phytologist

Research

ATR2^{Cala2} from *Arabidopsis*-infecting downy mildew requires 4 TIR-NLR immune receptors for full recognition

Dae Sung Kim[1,2], Yufei Li[2], Hee-Kyung Ahn[2], Alison Woods-Tör[3], Volkan Cevik[4], Oliver J. Furzer[2], Wenbo Ma[2], Mahmut Tör[3] and Jonathan D. G. Jones[2]

[1]State Key Laboratory of Biocatalysis and Enzyme Engineering, Hubei University, Wuhan, 430062, China; [2]The Sainsbury Laboratory, Norwich Research Park, Norwich, NR4 7UH, UK; [3]Department of Biological Sciences, School of Science and the Environment, University of Worcester, Worcester, WR2 6AJ, UK; [4]Department of Life Sciences, The Milner Centre for Evolution, University of Bath, Bath, BA2 7AY, UK

Authors for correspondence:
Jonathan D. G. Jones
Email: jonathan.jones@tsl.ac.uk

Mahmut Tör
Email: m.tor@worc.ac.uk

Received: *11 March 2024*
Accepted: *17 April 2024*

New Phytologist (2024)
doi: 10.1111/nph.19790

Key words: *Arabidopsis*, ATR2, *Hyaloperonospora arabidopsidis*, plant immunity, RPP2, RxLR effector, TNL.

Summary

- *Arabidopsis* Col-0 RPP2A and RPP2B confer recognition of *Arabidopsis* downy mildew (*Hyaloperonospora arabidopsidis* [*Hpa*]) isolate Cala2, but the identity of the recognized ATR2^{Cala2} effector was unknown.
- To reveal *ATR2^{Cala2}*, an F_2 population was generated from a cross between *Hpa*-Cala2 and *Hpa*-Noks1. We identified ATR2^{Cala2} as a non-canonical RxLR-type effector that carries a signal peptide, a dEER motif, and WY domains but no RxLR motif. Recognition of *ATR2^{Cala2}* and its effector function were verified by biolistic bombardment, ectopic expression and *Hpa* infection.
- ATR2^{Cala2} is recognized in accession Col-0 but not in Ler-0 in which RPP2A and RPP2B are absent. In *ATR2^{Emoy2}* and *ATR2^{Noks1}* alleles, a frameshift results in an early stop codon. RPP2A and RPP2B are essential for the recognition of ATR2^{Cala2}. Stable and transient expression of *ATR2^{Cala2}* under 35S promoter in *Arabidopsis* and *Nicotiana benthamiana* enhances disease susceptibility.
- Two additional Col-0 TIR-NLR (TNL) genes (*RPP2C* and *RPP2D*) adjacent to *RPP2A* and *RPP2B* are quantitatively required for full resistance to *Hpa*-Cala2. We compared *RPP2* haplotypes in multiple *Arabidopsis* accessions and showed that all four genes are present in all ATR2^{Cala2}-recognizing accessions.

Introduction

Plants, like animals, are constantly exposed to potentially damaging pathogens, and like invertebrates but unlike mammals, rely solely on innate immunity (Jones & Takemoto, 2004). The plant immune response is highly effective but must be activated early to thwart pathogens, and activation requires detection of pathogen molecules by cell surface and intracellular immune receptors. Cell-surface receptors usually detect relatively conserved pathogen-associated molecular patterns and activate pattern-triggered immunity (PTI) (Monaghan & Zipfel, 2012; Boutrot & Zipfel, 2017). During plant–microbe co-evolution, pathogens evolved the ability to deliver effector proteins to host cells that suppress PTI, enabling pathogen growth (Feng & Zhou, 2012). In turn, plants evolved intracellular immune receptors, often encoded by resistance (*R*) genes, that either directly or indirectly detect the presence of pathogen effector proteins (Nürnberger *et al.*, 2004; Chisholm *et al.*, 2006; Jones & Dangl, 2006; Jones *et al.*, 2016) and activate effector-triggered immunity (Dodds & Rathjen, 2010; Dangl *et al.*, 2013). According to the gene-for-gene model, resistance is determined by matching pairs of plant *R*-genes and pathogen avirulence (*Avr*) genes. Recognized effectors are often referred to as Avr proteins. Intracellular recognition usually requires nucleotide-binding, leucine-rich repeat (NB-LRR or NLR) immune receptors. NLR activation results in an elevated immune response, characterized by generation of reactive oxygen species, cell wall fortification, activation of defence-associated genes and a localized cell death known as the hypersensitive response (HR) (Spoel & Dong, 2012). Many cases of matching *R* and *Avr* genes have been described (Bernoux *et al.*, 2011; Césari *et al.*, 2014; Ma *et al.*, 2020; Redkar *et al.*, 2023). However, in some examples, disease resistance against a pathogen isolate or recognition of an Avr protein requires the coordinate function of pairs of NLR genes (Eitas & Dangl, 2010). Recent detailed studies on the *Arabidopsis* TIR-NLR pair RRS1 and RPS4, and the rice coiled-coil (CC)-NLR pairs RGA4/RGA5 and Pik-1/Pik-2 reveal how such protein pairs function together. The paired partners interact physically to form a receptor complex in which each protein plays distinct roles in effector recognition or signalling activation, exemplifying a conserved mode of action of NLR pairs in diverse plants (Césari *et al.*, 2014; Sarris *et al.*, 2015; Ma *et al.*, 2018). Such gene pairs are often divergently transcribed. Interestingly, 10 of 11 pairs of Toll interleukin-1 receptor (TIR)-NLR genes

show a head-to-head configuration in *Arabidopsis* (Meyers *et al.*, 2003; Saucet *et al.*, 2021). Divergent transcription may assure balanced levels of the protein pair to meet a strict stoichiometric requirement to act together, possibly in a complex (Narusaka *et al.*, 2009). However, the *Arabidopsis RPP2* locus that confers resistance to downy mildew (Sinapidou *et al.*, 2004) comprises two genes, *RPP2A* and *RPP2B*, which are not divergently transcribed.

In *Arabidopsis*, rice and many other plants, canonical and non-canonical R-Avr interactions have been found in response to a variety of microbial pathogens. Large-scale sequencing, genomics and rapid gene isolation techniques have accelerated the isolation of race-specific *R*-genes and their corresponding *Avr* (recognized effector) genes in *Triticeae*, including wheat, barley, rye and their wild relatives. Non-canonical NLR protein-coding genes with unique domain architectures have been found controlling race-specific resistance (Sánchez-Martín & Keller, 2021). Genetic studies of the flax–flax rust interaction identified four *R*-gene loci in flax that encode TIR–NLR and corresponding recognized effector genes, which encode small-secreted proteins with no locus similarity and no close homologues (Ellis *et al.*, 2007). The world's third-largest food crop, potato, severely suffers from late blight caused by oomycete, *Phytophthora infestans*. This oomycete secretes host-translocated RxLR effectors, some of which are avirulence factors that are recognized by NLR proteins from wild *Solanum* species (Vleeshouwers *et al.*, 2011; Lin *et al.*, 2023).

Downy mildews are obligate biotrophic oomycete pathogens that can cause significant economic impacts on crop and ornamental plants (Thines & Kamoun, 2010; Tör *et al.*, 2023). Downy mildew disease control is dependent on integrated strategies, incorporating cultural practices, deployment of resistant cultivars, crop rotation, systemic pesticides and biopesticides. However, downy mildews deploy large repertoires of effectors, including the so-called RxLR proteins that promote virulence or are recognized as avirulence factors (Baxter *et al.*, 2010; Tör *et al.*, 2023). *Hyaloperonospora brassicae* causes severe disease in Chinese cabbage (*Brassica rapa* L. ssp. *pekinensis*), which is native to China and is one of the most important vegetables in Asia. In epidemic seasons with warm temperatures and high humidity, 80–90% of Chinese cabbage plants are infected by *H. brassicae*, leading to a 30–50% reduction in production (Li *et al.*, 2011). Downy mildew caused by *Bremia lactucae* is the most important disease in lettuce (*Lactuca sativa* L.) reducing yield and decreasing the quality of the marketable portion (Parra *et al.*, 2021). Downy mildew caused by *Plasmopara viticola* can lead to severe damage to grapevines (Li *et al.*, 2015). Cucumber (*Cucumis sativus* L.) downy mildew, caused by *Pseudoperonospora cubensis*, is a major destructive and widespread disease of cucumber plants (Zhang *et al.*, 2019). There has been an increasing interest in the molecular mechanisms of downy mildew resistance (Liu *et al.*, 2021). The use of cultivars carrying dominant resistant (*Dm*) genes in lettuce is the most effective way to control downy mildew caused by *B. lactucae* (Parra *et al.*, 2021). The model plant *Arabidopsis* is susceptible to the downy mildew *Hyaloperonospora arabidopsidis* (*Hpa*) (Slusarenko & Schlaich, 2003). Various *Resistance to Peronospora parasitica* (*RPP*; the former name of *Hpa*) genes in different accessions confer resistance to specific *Hpa* isolates (Asai *et al.*, 2018).

Obligate biotrophic pathogen races or isolates differ in their capacity to evade or suppress host recognition (Oliver & Ipcho, 2004). Many oomycete pathogens deploy effector proteins with a signal peptide and typically the signature amino acid motifs RxLR and DEER (Rehmany *et al.*, 2005). A subset of such effectors also carries a variable number of repeats of a WY domain (Win *et al.*, 2012). RxLR effectors have been intensively investigated since their discovery (Anderson *et al.*, 2015; Wood *et al.*, 2020). RxLR genes are abundant in the genomes of *Phytophthora* and downy mildew species. Annotations based on canonical RxLR motifs predict that *Phytophthora* genomes typically contain several hundred RxLR genes (Anderson *et al.*, 2015).

The *Arabidopsis*|*Hpa* pathosystem reveals extensive genetic diversity in host *Resistance* (*RPP*) and cognate pathogen *ATR* (*Arabidopsis thaliana* recognized) genes, which encode *Hpa* avirulence factors (Coates & Beynon, 2010; Asai *et al.*, 2018). Using an *Hpa* reference genome (Baxter *et al.*, 2010), 475 *Hpa* gene models were identified that encode effector candidates in *Hpa*-Emoy2, using the following criteria: (1) proteins with a signal peptide and canonical RxLR motif, such as ATR1, ATR13 and ATR39 (HaRxLs) (Allen *et al.*, 2004; Rehmany *et al.*, 2005; Goritschnig *et al.*, 2012), (2) RxLR-like proteins with at least one non-canonical feature, such as ATR5 (HaRxLLs) (Bailey *et al.*, 2011), (3) putative Crinkler-like proteins with RxLR motif (HaRxLCRNs) (Win *et al.*, 2007) and (4) homologous proteins based on amino acid sequence similarity over the N-terminal region including a signal peptide and RxLR motif (e.g. HaRxL1b, HaRxLL2b and HaRxLCRN3b) (Asai *et al.*, 2014).

Several *RPP* genes, including *RPP1*, *RPP2A* and *RPP2B*, *RPP4*, *RPP5*, *RPP8*, *RPP13* and *RPP39* encode NLR immune receptors (Holub, 2008). Genetic analyses of avirulence in *Hpa* has confirmed a gene-for-gene relationship for *ATR* genes (Holub *et al.*, 1994) with their corresponding *RPP* genes. Recognized *Hpa* effectors ATR1, AvrRPP4, ATR5, ATR13 and ATR39 have been identified for RPP1, RPP4, RPP5, RPP13 and RPP39 (Allen *et al.*, 2004; Rehmany *et al.*, 2005; Bailey *et al.*, 2011; Goritschnig *et al.*, 2012; Asai *et al.*, 2018). For example, the *RPP1* locus, which contains a complex resistance gene cluster, was originally identified in *Arabidopsis* accession Wassilewskija (Ws-2) (Botella *et al.*, 1998). Several members of the *RPP1* gene family confer resistance against isolates of *Hpa* (Botella *et al.*, 1998; Rehmany *et al.*, 2005; Sohn *et al.*, 2007) including *RPP1*-WsA, *RPP1*-WsB, *RPP1*-WsC and *RPP1*-NdA, while *RPP1*-like genes from other accessions have been implicated in hybrid incompatibility (Bomblies *et al.*, 2007). Proteins encoded by two *RPP1* alleles have been shown to recognize the cognate effector ATR1 from *Hpa* (Rehmany *et al.*, 2005; Krasileva *et al.*, 2010; Ma *et al.*, 2020). The R proteins RPP1-WsB and RPP1-NdA share a common TNL domain architecture and are 87% identical at the amino acid level. Although polymorphisms are present throughout their coding sequences, most of the differences occur in the LRR region and include both single amino acid polymorphisms and short insertions and deletions. ATR1 belongs

to a simple locus in *Hpa* with allelic variants present in different pathogen races (Rehmany *et al.*, 2005; Krasileva *et al.*, 2010). ATR1 carries an N-terminal eukaryotic signal peptide and an RxLR motif (Rehmany *et al.*, 2005; Birch *et al.*, 2006) and associates with its cognate RPP1 immune receptor via its LRR domain (Krasileva *et al.*, 2010). The tetrameric complex containing four RPP1 and four ATR1 molecules is mediated by direct binding of ATR1 to a C-terminal jelly-roll/Ig-like domain (C-JID) and the LRRs of RPP1 (Ma *et al.*, 2020).

RPP2A and RPP2B are both required for resistance to *Hpa* isolate Cala2 (Sinapidou *et al.*, 2004), but their cognate effector ATR2 was not identified previously. Adjacent to *RPP2A* (*At4g19500*) and *RPP2B* (*At4g19510*) (Sinapidou *et al.*, 2004) lie two other TNL encoding genes (*At4g19520* and *At4g19530*, hereafter *RPP2C* and *RPP2D*). They comprise, in a head-to-head conformation, a similar gene pair to RRS1 and RPS4, including a C-terminal-extended post-LRR domain. In this research, we aimed to clone and characterize *ATR2* and investigate its virulence function and its contribution to effector recognition by the four genes at the *RPP2* locus.

Using an F_2 population generated from a cross between *Hpa*-Cala2 and *Hpa*-Noks1 (Bailey *et al.*, 2011), we positionally cloned *ATR2*. We show here that functional ATR2 is absent from the reference Emoy2 genome and its annotated proteome, that ATR2 confers elevated disease susceptibility when expressed *in planta* and that all four RPP2 paralogs contribute to its full recognition.

Materials and Methods

Plant materials and growth

Arabidopsis accessions, Col-0, Ler-0, Oy-0, Ws-2, Ws-2 *eds1* and CW84, which is an *Hpa*-susceptible recombinant inbred line generated from a cross between Col-0 and Ws-2 (Botella *et al.*, 1998) were grown at 22°C under short-day condition (10 h : 14 h, light : dark) and *Nicotiana benthamiana* plants were grown at 25°C under a 16 h : 8 h, light : dark period in environmentally controlled growth cabinets.

Positional cloning of $ATR2^{Cala2}$

The crossing of *Hpa*-Cala2 and *Hpa*-Noks1 and production of F_2 mapping population from a single-spored CaNo F1 were described previously (Bailey *et al.*, 2011). Initially, segregating 52 random CaNo F_2 isolates were bulked up on Ws-*eds1* seedlings and tested on Col-5 to determine the genetic nature of *ATR2*. As the genomic sequences of parental isolates were not available then, a similar approach to clone *ATR5* (Bailey *et al.*, 2011) was taken where DNA was isolated from individual CaNo F_2 isolates and a bulk segregant analysis was employed to clone *ATR2*. Two different bulks were constructed from the CaNo F_2 individuals (18 F_2s with *ATR2*/± and 17 with *atr2*/*atr2* genotypes), and AFLP was carried out with *Eco*RI and *Mse*I primer pairs as described (Bailey *et al.*, 2011). Fifteen polymorphic AFLP fragments were identified and converted to CAPS markers to map *ATR2* onto publicly available BAC contigs. As the *Hpa*-Emoy2 reference genome became available, we used these markers to identify the *Hpa*-Emoy2 SuperContig9. As the number of recombinants were very low, additional CaNo F_2 isolates were generated, and Illumina paired-end sequencing data of CaNo F_2 bulks were obtained. As the genomic data for *Hpa*-Cala2 and *Hpa*-Noks1 became available (Woods-Tör *et al.*, 2018), the bulk sequences were mapped onto *Hpa*-Cala2 genome as described (Woods-Tör *et al.*, 2018) and SNP markers were identified within the interval. Further markers were generated from the identified SNP sites, and using a total of 130 CaNo F_2 isolates, we mapped *ATR2* to a 186.5 kb interval on *Hpa*-Cala2 SuperContig9. Further markers were generated and new F_2 isolates were obtained, and the locus was mapped to a 112 kb interval. We compared genomic sequences of *Hpa*-Emoy2, *Hpa*-Noks1and *Hpa*-Cala2 for the interval to identify possible candidates for *ATR2*. All PCR amplifications for mapping were performed as described (Woods-Tör *et al.*, 2018).

Pathogen assays

Hpa isolates, *Hpa*-Emoy2, *Hpa*-Noks1 and *Hpa*-Cala2, were propagated and maintained by weekly sub-culture on 14-d-old *Arabidopsis* seedlings. Preparation of inoculum for experiments and the assessment of sporulation were as described previously in Bailey *et al.* (2011).

Pseudomonas syringae pv *tomato* (*Pst*) DC3000 was grown in King's B broth (10 g peptone, 15 g glycerol, 1.5 g K_2HPO_4 and 5 mM $MgSO_4$ per litre) containing 50 μg ml^{-1} rifampicin. Leaves of 5-wk-old *Arabidopsis* plants were infiltrated with 10^5 CFU ml^{-1} of *Pst* DC3000 using a needleless syringe. Bacterial growth was measured at 0- and 3-d post inoculation (dpi).

Phytophthora infestans isolate 88069 was grown on Rye Agar at 19°C for 2 wk. Plates were flooded with 5 ml of cold H_2O and scraped with a glass rod to release zoospores. The resulting solution was collected in a falcon tube and zoospore numbers were counted using a hemacytometer and adjusted to 2×10^4 zoospores ml^{-1} and 10 μl droplets were inoculated onto the abaxial side of leaves of intact *N. benthamiana* plants. Inoculated leaves were then stored on moist tissues in sealed boxes.

Plasmid construction

All the constructs used in this study were generated using Uracil-Specific Excision Reagent (USER) enzyme cloning method (Geu-Flores *et al.*, 2007). Briefly, target DNA to be cloned into destination USER vectors, pICSLUS0003 or pICSLUS0004 (archived in The Sainsbury Laboratory) was amplified using *PfuTurbo*® C_x polymerase (Agilent Technologies, Santa Clara, CA, USA) with uracil-containing primer pair then assembled with desired tag ('Hellfire' including 6-His and 3-FLAG epitopes), linearized vector and USER enzyme (NEB, Ipswich, MA, USA). For transient gene expression in *N. benthamiana* or *Nicotiana tabacum*, *ATR2* candidates without signal peptide were cloned and assembled.

Bombardment and luciferase assays

Co-bombardment assays were performed as described previously with some modifications (Bailey *et al.*, 2011). Briefly, *Arabidopsis* plants were grown with short-day condition until 6 wk old. Detached leaves were placed on a 1% MS agar in a Petri dish. One micrometre of tungsten particles was coated with the plasmids carrying genes *ATR2* and luciferase under 35S promoter. Bombardments were performed using a Bio-Rad PDS-1000 (He) apparatus with 1100 p.s.i. rupture discs, as per the manufacturer's instructions. For each replicate, a leaf from both test and control plant genotypes were co-bombarded together in a single shot. Bombarded leaves were put into 10-ml plastic vials filled with water 1 cm from the bottom and were incubated at 25°C for 20 h.

For the luciferase assay, a Dual Reporter Luciferase Assay system (Promega, Madison, WI, USA) was used. Four transiently bombarded leaf events were pooled together and crushed in Luciferase Cell Culture Lysis buffer (Promega). The extract was centrifuged at 11 269 ***g***-force for 10 min at 4°C. Twenty microlitres of the lysate was then dispersed in 96-well plates in triplicates and analysed on Varioskan Flash Instrument (Thermo Fisher Scientific, Waltham, MA, USA) by injecting 100 µl of luciferase assay reagent II, which includes substrate and reaction buffer. A 10-s read time was used to measure luciferase activity for each well.

Expression analysis

Total RNA was isolated from three biological replicates using the RNeasy Plant Mini Kit (Qiagen, Hilden, Germany) with the Dnase treatment (Qiagen). cDNA was synthesised using SuperScript IV Reverse Transcriptase (Thermo Fisher Scientific). For *ATR2* gene expression analysis during *Hpa* infection, reverse transcription polymerase chain reaction (RT-PCR) was performed.

Transient expression in *Nicotiana* species

Agrobacterium tumefaciens GV3101 strain harbouring *ATR2* candidate fused to 35S promoter was streaked on selective media and incubated at 28°C for 24 h. A single colony from the streaked inoculum was transferred to liquid LB media with appropriate antibiotic and incubated at 28°C for 48 h in a shaking incubator at 5 ***g***-force. The cultures were centrifuged at 2012 ***g***-force for 5 min and resuspended in infiltration buffer (10 mM $MgCl_2$, 10 mM MES, pH 5.7), and acetosyringone was added to a final concentration of 200 µM at OD_{600} of 1.0. The abaxial surface of 4-wk-old *N. tabacum* or *N. benthamiana* was infiltrated with a 1-ml needleless syringe (Kim *et al.*, 2015).

Arabidopsis transformation

Arabidopsis accessions Col-0 and Ler-0 expressing *ATR2* candidate gene, and CW84 expressing Col-*RPP2* cluster harbouring JAtY clone (Zhou *et al.*, 2011), were transformed using *A. tumefaciens* strain GV3101 by flower dipping method (Clough & Bent, 1998).

RPP2 cluster haplotype analyses

Full-length amino acid sequences of individual RPP2A, RPP2B, RPP2C and RPP2D from 64 different *Arabidopsis* accessions were extracted from pan-NLRome data (Van de Weyer *et al.*, 2019). Each group of RPP2 was aligned to each other using the Geneious Prime software to investigate haplotype patterns of RPP2 clusters. Pfam (Punta *et al.*, 2012; http://pfam-legacy.xfam.org) was used for domain analysis in RPP2 cluster.

Protein structure modelling

Protein tertiary structure model of full-length $ATR2^{Cala2}$ was generated by Alphafold 2 (Jumper *et al.*, 2021; Varadi *et al.*, 2021). The region spanning the Y-WY sequences was extracted and superimposed with the structure of full-length PsPSR2 using PyMOL Molecular Graphics System, v.1.2r3pre, LLC (Xiong *et al.*, 2014; He *et al.*, 2019; Hou *et al.*, 2019). Secondary structures and surface accessibility of $ATR2^{Cala2}$ were predicted by NetSurfP-3.0 (Høie *et al.*, 2022). Alignment with published LWY effectors revealed the conserved W and Y residues in $ATR2^{Cala2}$ and the corresponding Y and WY modules (He *et al.*, 2019).

Accessions

Genomic sequences of parental isolates can be found under accession nos. GCA_001414265.1 for *Hpa*-Cala2, GCA_001414525.1 for *Hpa*-Noks1 and GCA_000173235.2 for *Hpa*-Emoy2 in NCBI. The raw sequence reads from the genomics sequencing of bulks are available from the Sequenced Read Archive (SRA) under accession nos. SRX13788375 (avirulent) and SRX13788374 (virulent). $ATR2^{Cala2}$ and $ATR2^{Emoy2}$ sequences were deposited in NCBI (GenBank accession nos. ON994189 and ON994190, respectively). Resistance (*R*) gene sequence capture (RenSeq) raw sequencing data of FN2 (*rpp2a-1*) mutant is available from the SRA (accession no. PRJNA955397).

Supporting Information Methods S1 contains additional methods, including protein gel blot, R gene sequence capture (RenSeq), and bioinformatics.

Results

Mapping *ATR2*

Positional cloning was used to identify the *ATR2* locus in *Hpa*-Cala2. A segregating CaNo F_2 population (Bailey *et al.*, 2011) was used to define the *ATR2* locus. Initially, 52 randomly chosen F_2 isolates were tested on Col-5. A single semi-dominant avirulence determinant designated $ATR2^{Cala2}$ segregated in the F_2 population (avirulence : virulence ratio was 40 : 12, with chi-square = 0.1025 and $P = 0.74$; Table S1). Bulked segregant analysis was used to identify AFLP markers that are linked to *ATR2* in the CaNo F_2 population. AFLP markers were cloned and converted to CAPS markers, which were then used for mapping *ATR2*. The reference genome of *Hpa*-Emoy2 was still being

generated during this early mapping work, and genomic sequence data for *Hpa*-Cala2 and *Hpa*-Noks1 were not available. Once *Hpa*-Emoy2 genomic sequence became available, we transferred the AFLP-derived CAPS markers to *Hpa*-Emoy2 SuperContig9, which helped us to identify the physical location of the locus (Figs S1, S2).

We then generated 100 bp paired-end Illumina HiSeq2500 sequencing data from the two newly bulked (virulent and avirulent) pools, comprising 110 million reads for the virulent bulk and 104 million reads for the avirulent bulk. We also utilized *Hpa*-Cala2 and *Hpa*-Noks1 genomic sequences (Woods-Tör *et al.*, 2018) to identify SNPs between *Hpa*-Cala2 and *Hpa*-Noks1 genomes. Using new markers generated from these SNPs, we established an interval of 186.5 kb on *Hpa*-Emoy2 SuperContig9: 656515–843042 (Fig. S1). We generated further markers and F_2 isolates and narrowed the *ATR2* locus to a 112 kb interval on *Hpa*-Emoy2 SuperContig9: 708503–820527 (Tables 1, S2). Genes in the *ATR2* interval encode effector-like proteins (Results S1; Figs S2–S4).

$A2C3^{Cala2}$ encodes an RxLR effector-like candidate for $ATR2^{Cala2}$

A2C3 was identified in *Hpa*-Cala2 after re-sequencing of the 5 kb upstream of *A2C1* and *A2C2*, which includes a highly polymorphic region of Cala2 compared with Emoy2 (Fig. 1a). We found a transposable element in this region of the *Hpa*-Emoy2 genome and a 2.3 kb deletion in *Hpa*-Cala2. We also found a cytosine insertion on the *Hpa-802071* coding region in Cala2, which created a frameshift in the *Hpa-802071* coding region (Fig. 1b). To determine whether $A2C3^{Cala2}$ co-segregates with recognition by *RPP2* in the F_2 population, *A2C3* alleles were amplified and sequenced from 12 CaNo F_2 segregants, *Hpa*-Emoy2, *Hpa*-Noks1 and *Hpa*-Cala2 (Fig. S5). All avirulent F_2s were homozygous or heterozygous for $A2C3^{Cala2}$, while all virulent F_2s were homozygous for $A2C3^{Emoy2/Noks1}$ (Figs 1c, S5c). Of *Hpa*-Emoy2, *Hpa*-Noks1 and *Hpa*-Cala2, only *Hpa*-Cala2 carries this non-canonical RxLR effector candidate ($A2C3^{Cala2}$), which has a signal peptide, a dEER, and Y and WY motifs (Figs 2a, S6a). $A2C3^{Emoy2}$ and $A2C3^{Noks1}$ alleles were identical to each other with early stop codons caused by a frameshift. These data suggested $A2C3^{Cala2}$ might be $ATR2^{Cala2}$. We analysed synonymous and non-synonymous SNPs in *A2C3* alleles among seven different *Hpa* isolates for which genomic data are available. Ten non-synonymous SNPs are found only in *Hpa*-Cala2, indicating specificity of $A2C3^{Cala2}$ (Table S3). Alignment of $A2C3^{Cala2}$ with *Phytophthora* LWY effectors revealed conserved W and Y residues and the corresponding Y and WY modules of $A2C3^{Cala2}$ (He *et al.*, 2019). The Y–WY modules of $A2C3^{Cala2}$ in an $A2C3^{Cala2}$ structural model predicted by Alphafold 2 were extracted and superimposed with PsPSR2, which is a typical RxLR effector with one WY motif and six LWY motifs. This region was well-matched on PsPSR2 Y5-LWY6 (region from Y5 of LWY5 to LWY6) with Root Mean Square Deviation

Table 1 Intervals of *ATR2* from CaNo F_2 isolates. Red: Cala2 homozygote; Yellow: Noks1 homozygote; Orange: Cala2-Noks1 heterozygote at *A2C3*.

Isolate F2	Marker[a] 656515	708503	759570	801023	820527	826062	843042	Col-0 Phenotype[b]
Cala2	Cala2[c]	Cala2	Cala2	Cala2	Cala2	Cala2	Cala2	Av
Noks1	Noks1[d]	Noks1	Noks1	Noks1	Noks1	Noks1	Noks1	V
2	Noks1/Cala2[e]						Noks1/Cala2	Av
9	Noks1/Cala2						Noks1/Cala2	Av
10	Noks1/Cala2						Noks1/Cala2	Av
15	Noks1/Cala2						Noks1/Cala2	Av
21	Cala2						Cala2	Av
30	Cala2	Noks1/Cala2	Noks1/Cala2	Noks1/Cala2	Noks1/Cala2	Noks1/Cala2	Noks1	Av
34	Noks1/Cala2	Cala2	Cala2	Cala2			Cala2	Av
45	Noks1	Cala2	Cala2	Cala2			Cala2	Av
104	Noks1						Noks1	V
113	Noks1	Noks1	Noks1	Noks1	Noks1	Noks1	Noks1/Cala2	V
118	Noks1						Noks1	V

[a]Each marker number indicates nucleotide no. on SuperContig9 from Emoy2 genomic sequence as a reference.
[b]Virulent (V) or avirulent (Av) on Col-0.
[c]Cala2 homozygote.
[d]Noks1 homozygote.
[e]Cala2-Noks1 heterozygote.

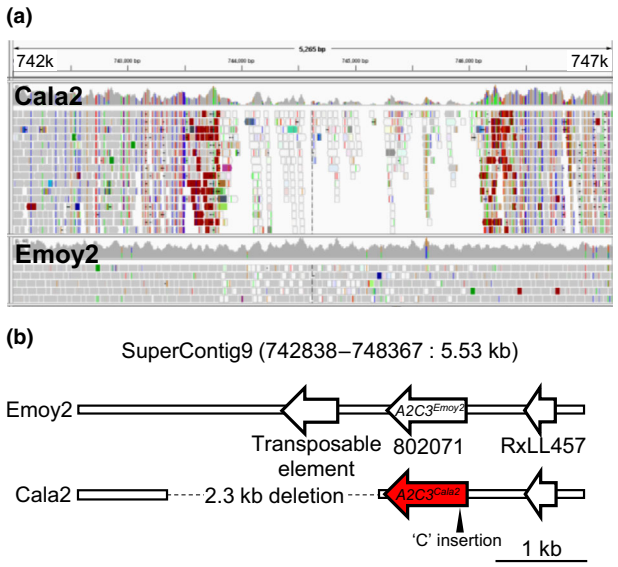

(c)

Isolate F_2	Homozygosity on *A2C3*	Col-0 Phenotype	Marker 746974
Cala2	Cala2	Av	CACC**C**GGT
Noks1	Noks1	V	CACC–GGT
2	Noks1/Cala2	Av	CACC(**C**/G)G(G/T)(T/C)
9	Noks1/Cala2	Av	CACC(**C**/G)G(G/T)(T/C)
10	Cala2	Av	CACC**C**GGT
15	Noks1/Cala2	Av	CACC(**C**/G)G(G/T)(T/C)
21	Cala2	Av	CACC**C**GGT
30	Noks1/Cala2	Av	CACC(**C**/G)G(G/T)(T/C)
34	Cala2	Av	CACC**C**GGT
45	Cala2	Av	CACC**C**GGT
104	Noks1	V	CACC–GGT
113	Noks1	V	CACC–GGT
118	Noks1	V	CACC–GGT

Fig. 1 Genetic determination of *A2C3*^{Cala2} co-segregation from avirulent F_2 isolates. (a) Comparison of polymorphic region of Cala2 with Emoy2 from 742k to 747k of SuperContig9. Screenshot was captured from the IGV software. (b) Transposable element next to '802071' on Emoy2 and 2.3 kb deletion on Cala2 of assigned region. *A2C3*^{Cala2} allele is highlighted with red colour. A cytosine (C) insertion at 746974 indicated with a black triangle. (c) Analyses of homo- or heterozygosity, avirulent (Av) or virulent (V) on Col-0 and a segregated cytosine (C) insertion in Av isolates at the frameshift region (746974) by sequencing from Supporting Information Fig. S5. Red: Cala2 homozygote; Yellow: Noks1 homozygote; Orange: Cala2-Noks1 heterozygote at *A2C3*. Inserted cytosine was bold highlighted.

(RMSD) = 2.305 (Fig. 2b). This structural comparison also revealed that there is an L-like module that harbours several leucines (L) contributing to the additional hydrophobic core formation between Y and WY modules of A2C3^{Cala2} even though this was not predicted by amino acid sequence comparison (Figs 2b, S6b).

To reveal whether A2C3^{Cala2} has weighted sequence similarity to other RxLR proteins in the post-SP and pre-WY region, a Hidden Markov Model was used using 475 published *Hpa* effectors including RxLR, RxLL and CRN effectors. No aligned sequences of *A2C3*^{Cala2} were found likely due to the diversification of N-terminal sequences of *Hpa* effectors. Therefore, we constructed a phylogenetic tree using post-SP N-terminal sequences of 476 *Hpa* effectors including A2C3^{Cala2} and found only a few effectors cluster in a clade with A2C3^{Cala2}. Even ATR5, another non-RxLR effector, is not related with A2C3^{Cala2}, and previously defined ATR effectors are distributed throughout the tree indicating there is no specific signature in N-terminal sequences of *Hpa* effectors (Fig. S7).

We determined the expression of *A2C3*^{Cala2} alleles during *Hpa* infection. *Arabidopsis* Oy-0 accession was infected with *Hpa*-Emoy2 and Ler-0 was infected with *Hpa*-Cala2, and Col-*eds1* was used as hyper-susceptible control. *A2C3*^{Cala2} is expressed at 3 dpi (Fig. S8a). Previously, Asai *et al.* (2014) performed expression profiling of *Hpa* genes from *Hpa* Emoy2. RNA-seq data of *Hpa-802071* (*A2C3*$^{Emoy2/Noks1}$) were retrieved from the data. Again, *A2C3*$^{Emoy2/Noks1}$ is induced after infection and shows the highest expression at 3 dpi (Fig. S8b). We proceeded to further evaluate the *A2C3*^{Cala2} allele as a strong candidate for *ATR2*^{Cala2}.

A2C3^{Cala2} triggers defence in Col-0

When luciferase assays were performed to evaluate the recognition of A2C3^{Cala2} in *Arabidopsis*, a reduction of at least fivefold in luciferase activity was detected in Col-0 compared with empty vector (EV) control. Equal luciferase activity was detected in an *Hpa*-susceptible recombinant inbred line *Arabidopsis* CW84 when leaf tissue was bombarded with 35S:*A2C3*^{Cala2} or EV. These results suggest that Col-0 but not CW84 can recognize A2C3^{Cala2}. As before, CCG28 was recognized by WRR4A, which served as a positive control (Fig. 2c) (Redkar *et al.*, 2023). Thus, our genetic investigations and bombardment experiments are consistent with A2C3^{Cala2} being the avirulence determinant ATR2^{Cala2}, and we hence refer to A2C3^{Cala2} as ATR2^{Cala2}. As an additional test of ATR2^{Cala2} detection by RPP2 in *Arabidopsis*, *ATR2*^{Cala2} under 35S promoter was transformed into Col-0. Only three T_1 lines were selected from antibiotic screening, and strikingly, all three transformants showed strong dwarf phenotype, consistent with recognition of *ATR2*^{Cala2} in *Arabidopsis* Col-0 background (Fig. 2d).

ATR2^{Cala2} enhances susceptibility in the absence of host recognition

Plant pathogen effector proteins that are translocated into host cells can attenuate host defence. Many pathogen effectors interfere with cellular processes that are essential for innate immunity.

To evaluate its virulence function, *ATR2*^{Cala2} was transiently expressed in *N. benthamiana* leaves that were then inoculated with *P. infestans* race 88069. The *P. infestans* lesion area was

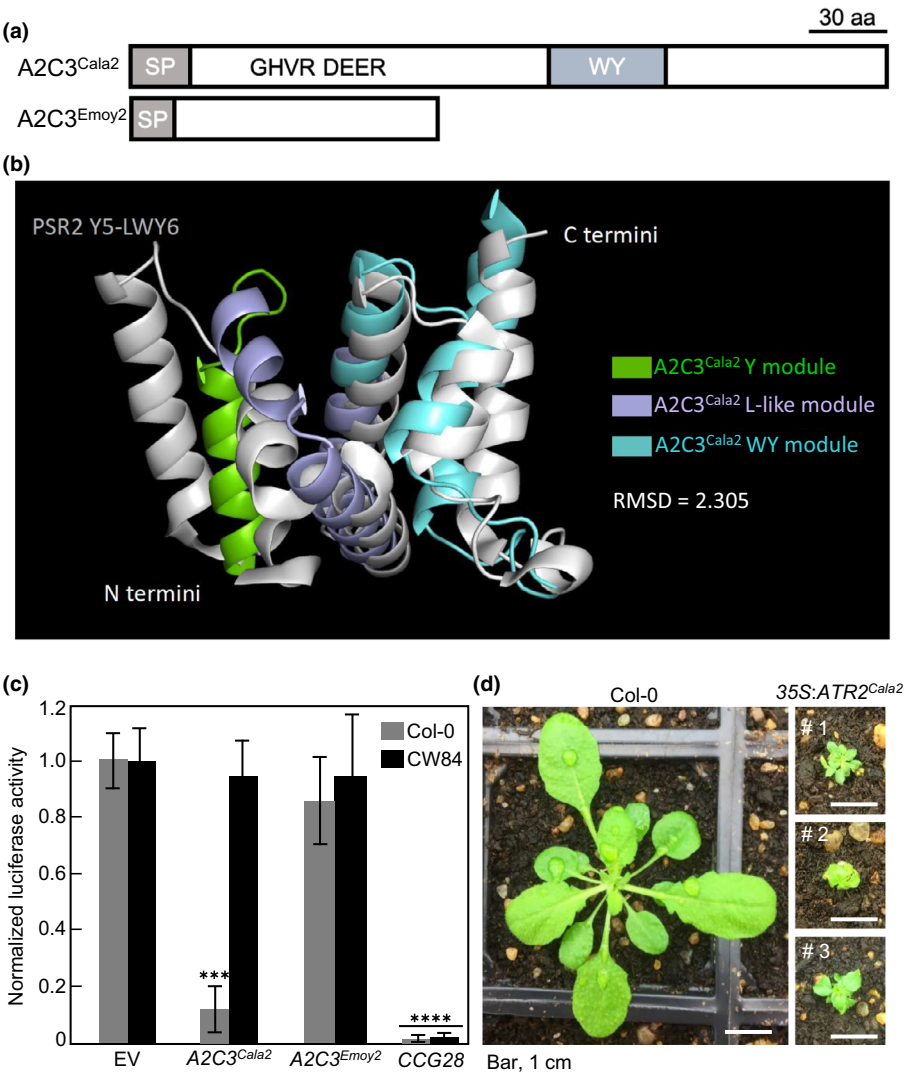

Fig. 2 A2C3^{Cala2} recognition capacity in Col-0. (a) Schematic diagrams of A2C3 of *Hpa* Cala2 and Emoy2. (b) Alphafold 2 prediction of Y and WY modules of A2C3^{Cala2}, and super-imposition with PsPSR2. PsPSR2 contains seven (L)WY units with Y5-LWY6 showing the highest similarity with A2C3^{Cala2}. This structural comparison also revealed an 'L'-like fold between the 'Y' and 'WY' sequence in A2C3^{Cala2}. (c) Biolistic bombardment of *A2C3* with luciferase into Col-0 and CW84 in which RPP2 is absent. CCG28 recognized by WRR4A in Col-0 and CW84 served as a positive control. Data are mean ± SD from three independent experiments. Asterisks (***, $P < 0.001$; ****, $P < 0.0001$) indicate statistical significance compared with luciferase alone in Col-0 or CW84 by two-way ANOVA with Tukey's multiple comparison test. EV, empty vector. (d) Transgenic Arabidopsis Col-0 expressing *ATR2*^{Cala2} under 35S promoter. Photographs were taken from the 4-wk-old plants under short-day condition. Bars, 1 cm.

significantly larger in *ATR2*^{Cala2}-expressing leaf sectors than in GFP vector control (Fig. 3a). At 7 dpi, lesion area in the *ATR2*^{Cala2}-expressing region was more than four times larger than that observed in GFP control region (Fig. 3b). Stable *ATR2*^{Cala2}-expressing *Arabidopsis* lines (35S:*ATR2*^{Cala2}) were generated in Ler-0, which lacks *RPP2A* and *RPP2B*. In contrast to *ATR2*^{Cala2} expressing Col-0, all transgenic lines selected grew similar to Ler-0 wild-type (WT; Fig. 3c). Strikingly, all the transgenic lines were more susceptible to virulent *Pst* DC3000 or *Hpa*-Cala2 compared with Ler-0 WT control (Fig. 3d,e). Ler-*eds1* was used as hyper-susceptible control. Collectively, these data show that in both *Arabidopsis* and *N. benthamiana*, *ATR2*^{Cala2} expression can compromise plant innate immunity in the absence of recognition by a cognate *R*-gene.

In addition to RPP2A and RPP2B, two additional linked TNLs, RPP2C and RPP2D, are required for full RPP2 function

We tested the requirement for *RPP2A* (*At4g19500*) and *RPP2B* (*At4g19510*) in ATR2^{Cala2} recognition. There are two other adjacent TIR-NB-LRR genes (*At4g19520* and *At4g19530*, hereafter *RPP2C* and *RPP2D*) (Fig. S9a) that comprise a gene pair similar to *RRS1* and *RPS4*, with C-terminal-extended post-LRR domains and a head-to-head orientation (Fig. S9a,b). RPP2A contains two TIR-NB-ARC domains connected by the *Arabidopsis* LSH1 and *Oryza* G1 (ALOG) domain followed by LRRs towards its C terminus. Post-LRR (PL) domains of RPP2B and RPP2D are homologous to the RPP1 C-terminal jelly-roll/Ig-like (C-JID) domain. RPP2C harbours an additional TIR domain following an extended post-LRR domain (Fig. S9b; Table S4). We obtained the fast neutron 2 (FN2) *rpp2a* mutant (Sinapidou *et al.*, 2004), and several T-DNA insertional mutants from GABI or SALK for *rpp2b*, *rpp2c* and *rpp2d* (Fig. S9c). We combined sequence capture with Illumina sequencing (RenSeq) with DNA from the FN2 (*rpp2a-1*) mutant and confirmed a 25 bp deletion in *RPP2A*. The *RPP2B*, *RPP2C* and *RPP2D* mutations were also verified (Fig. S10). After inoculating mutants with *Hpa*-Cala2, conidiospores were counted at 7 dpi. Ler-0 and Ws-*eds1* were used as susceptible controls. While fewer than 1×10^2 spores per plant were detected in the resistant Col-0, *c.* 4×10^3 spores per plant were detected on *rpp2a-1* and *rpp2b-1* mutants with

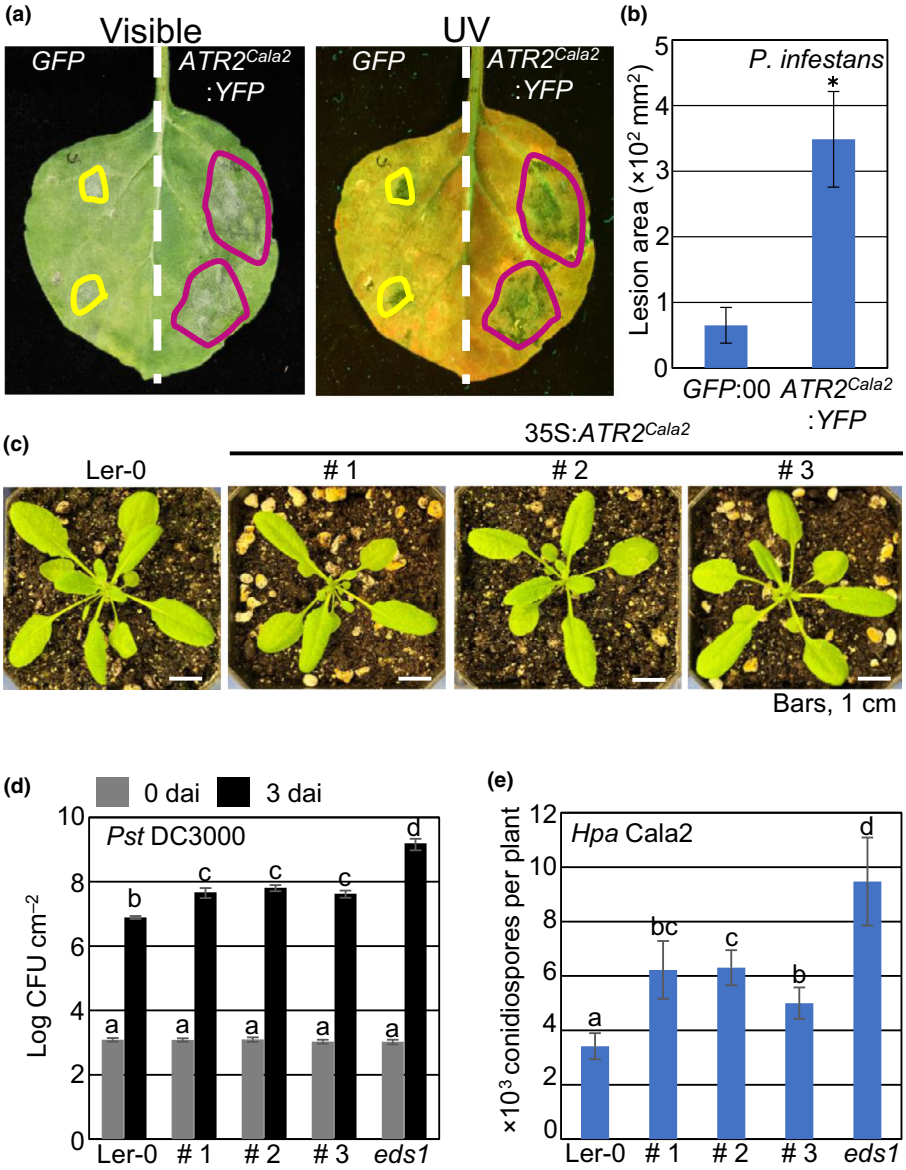

Fig. 3 Enhanced disease susceptibility resulting from exogenous *ATR2*^{Cala2} expression. (a) Phenotypes on *Nicotiana benthamiana* transiently expressing the *GFP* control (GFP) or *ATR2*^{Cala2}*:YFP* under the 35S promotor followed by *Phytophthora infestans* 88069 inoculation (2×10^4 zoospores ml^{-1}) 2 d after transient expression. Photographs were taken 7 days after inoculation (dai) with *P. infestans*. (b) Disease lesion area of *P. infestans* on *N. benthamiana* leaves. Forty lesion squares of each were measured. (c) Generation of constitutively *ATR2*^{Cala2} expressing transgenic Arabidopsis in Ler-0 background. Bars, 1 cm. (d) Bacterial growth in Ler-0, *ATR2*^{Cala2}-OX Ler-0 (# 1, # 2 and # 3) and Ws-*eds1* (*eds1*) as a hyper-susceptible control infected with *Pst* DC3000 (10^5 CFU ml^{-1}). (e) Quantification of conidiospores on wild-type and transgenic plants at 7 dai infected with *Hpa* Cala2 (5×10^4 conidiospores ml^{-1}). Data are means ± SD from three independent experiments. Asterisks indicate significant differences as determined by Student's *t*-test ($P < 0.05$). According to Fisher's Least Significant Difference ($P < 0.05$), statistical significance was shown by different letters above each bar.

similar values to those obtained from Ler-0 (near 4.8×10^3 per plant), indicating Cala2 resistance in Col-0 is compromised by *rpp2a* or *rpp2b* mutations (Fig. 4a). Interestingly, *rpp2c-1* and *rpp2d-1* mutants also showed compromised resistance to *Hpa*-Cala2. Around 1.2×10^3 to 1.3×10^3 spores per plant were counted from *rpp2c* and *rpp2d* mutants, suggesting *RPP2C* and *RPP2D* also contribute to full resistance against *Hpa*-Cala2 in Col-0 (Fig. 4a). Trailing necrosis was observed on *rpp2c* and *rpp2d* mutants, while no necrosis was observed on Col-0 at 6 dpi (Fig. S11a). To visualize cell death and hyphal growth, we performed trypan blue staining at 5 dpi using infected cotyledons. Local cell death was observed on Col-0, and hyphal growth and haustoria formation over the whole leaf was observed on *rpp2a*, *rpp2b* and Ler-0 cotyledons, as well as Ws-*eds1*. Partial but restricted hyphal growth was detected on *rpp2c* and *rpp2d* mutants (Fig. 4b).

Transgenic complementation assays with CW84 were carried out using JAtY 49E17 clone (Zhou *et al.*, 2011), which harbours the whole RPP2 cluster. While sporangiophore formation was observed on CW84, complemented transgenic plants restored complete resistance to *Hpa*-Cala2 (Fig. S11b). When *Hpa*-Emoy2 was inoculated onto *rpp2a*, *rpp2b*, *rpp2c* and *rpp2d* mutants, resistance was not compromised, due to *RPP4*-dependent resistance in Col-0 (van der Biezen *et al.*, 2002; Fig. S12), which is why the susceptible phenotypes were only seen after inoculation with *Hpa*-Cala2.

To assess *ATR2*^{Cala2} recognition capacity by RPP2 paralogs, luciferase eclipse assays were conducted using individual Col-0 *rpp2a-1*, *rpp2b-1*, *rpp2c-1* and *rpp2d-1* mutants. The luciferase activity was normalized to compare with that of EV control on Col-0 (Fig. 4c). The normalized luciferase activity in each individual Col-0 *rpp2a* mutant and Col-0 with EV was comparable

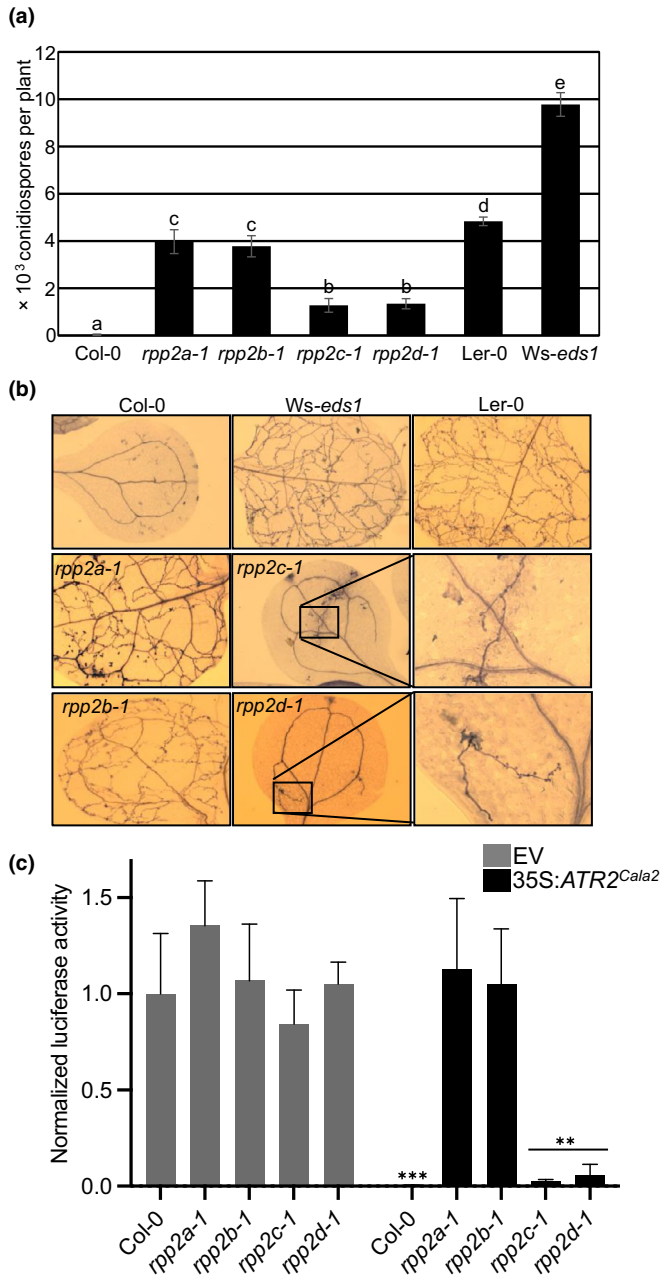

Fig. 4 Compromised *Hpa* Cala2 resistance in *rpp2* mutants.
(a) Quantification of conidiospores on Col-0, individual *rpp2* mutants from Col-0, Ler-0 and Ws-*eds1* at 7 days after inoculation (dai) infected with *Hpa* Cala2 (5×10^4 conidiospores ml^{-1}). Data are means ± SD from three independent experiments. According to Fisher's Least Significant Difference, ($P < 0.05$), statistical significance was shown by different letters above each bar. (b) Trypan blue staining of *Hyaloperonospora arabidopsidis* hyphal growth on cotyledons at 5 dai. Hyphal growth region on *rpp2c* and *rpp2d* mutants was enlarged to clearly show the *Hpa* hyphal development. (c) Luciferase measurement upon biolistic bombardment into Col-0 and *rpp2* mutants. Statistical significance compared with luciferase alone in Col-0 is indicated by asterisks (**, $P < 0.01$; ***, $P < 0.001$) according to two-way ANOVA with Tukey's multiple comparison test.

with no significant differences indicating particle bombardment distributed well through the leaves of Col-0 and each mutant. When *ATR2*^{Cala2} was bombarded together with 35S:*luciferase* on Col-0, normalized luciferase activity was strongly reduced, ranging from 0.004 to 0.007, while those on *rpp2a-1* or *rpp2b-1* still maintained a range of 0.86–1.55, indicating ATR2^{Cala2} recognition is almost completely abolished in *rpp2a-1* and *rpp2b-1* mutants. ATR2^{Cala2} was still recognized in *rpp2c-1* and *rpp2d-1* mutants, with normalized activity ranging from 0.01 to 0.1 (Fig. 4c). Even though no statistically significant differences were detected between *ATR2*^{Cala2}-bombarded Col-0, *rpp2c-1* and *rpp2d-1*, the average values of the luciferase activities on *rpp2c-1* (mean, 0.024) and *rpp2d-1* (mean, 0.054) are almost 5–10 times higher than on Col-0 (mean, 0.005) when co-bombarded with *ATR2*^{Cala2}, consistent with *RPP2C* and *RPP2D* weakly contributing to ATR2^{Cala2} recognition. These data indicate *RPP2C* and *RPP2D* are also required for full ATR2^{Cala2}-triggered immunity.

To monitor whether the co-expression of *RPP2A*, *RPP2B*, *RPP2C* and *RPP2D* with or without *ATR2*^{Cala2} can trigger HR, we transiently expressed *RPP2A*, *RPP2B*, *RPP2C* or *RPP2D*, either alone or co-expressing *RPP2A*/*RPP2B*, *RPP2C*/*RPP2D*, *RPP2A*/*RPP2B*/*RPP2C*/*RPP2D* or *RPP2A*/*RPP2B*/*RPP2C*/*RPP2D* in combination with *ATR2*^{Cala2} in *N. benthamiana*. *Rpi-amr3* and *Avramr3*, an *R*-gene from *Solanum americanum* and the recognized *P. infestans* RxLR *Avr* gene, respectively, were used as a HR-inducing positive control (Lin *et al.*, 2022). No auto-activity of any RPP combination was observed, either by individual *RPP2* paralogs or by co-expression of *RPP2* paralogs. Similarly, no HR was observed when all four *RPP2* were expressed in combination with *ATR2*^{Cala2} (Fig. S13). We performed co-immunoprecipitation (co-IP) to monitor whether ATR2^{Cala2} can interact with each RPP2 protein using *N. benthamiana* transient expression assays. However, under our experimental conditions, no association was detected between ATR2^{Cala2} and any RPP2 protein (Fig. S14). RPP2C protein was not detected by Western blot; we infer that more detailed work might be required to correctly define its splicing and thus where to attach an epitope tag to its C terminus. However, *RPP2C* expression was abundantly detected by reverse transcription polymerase chain reaction indicating that the TAIR annotation that we used to tag RPP2C (RPP2C.1) is probably wrong and did not enable us to express the protein in transient assays. Alternatively, *RPP2C* might be differentially spliced between *Arabidopsis* and *N. benthamiana* (Fig. S15).

RPP2 haplotype diversity

As the *RPP2* cluster containing *RPP2A*, *RPP2B*, *RPP2C* and *RPP2D* is required for full ATR2^{Cala2}-triggered resistance, we assessed *RPP2* haplotype diversity in multiple *Arabidopsis* accessions. An investigation of the *Arabidopsis* pan-NLRome (Van de Weyer *et al.*, 2019) enabled in-depth analysis for the *RPP2* cluster. We compared the *RPP2* cluster in 64 *A. thaliana* accessions (Fig. S16). Col-0, Oy-0 and Can-0 have the complete form of the *RPP2* cluster, while other accessions lack some *RPP* genes or harbour incomplete (partial) *RPP* genes (Fig. 5a). Interestingly, almost all accessions contain a complete form of *RPP2B*, and seven ecotypes among 21 harbour *RPP2A* while many of other ecotypes have incomplete alleles of *RPP2A* (Fig. 5a). Almost half

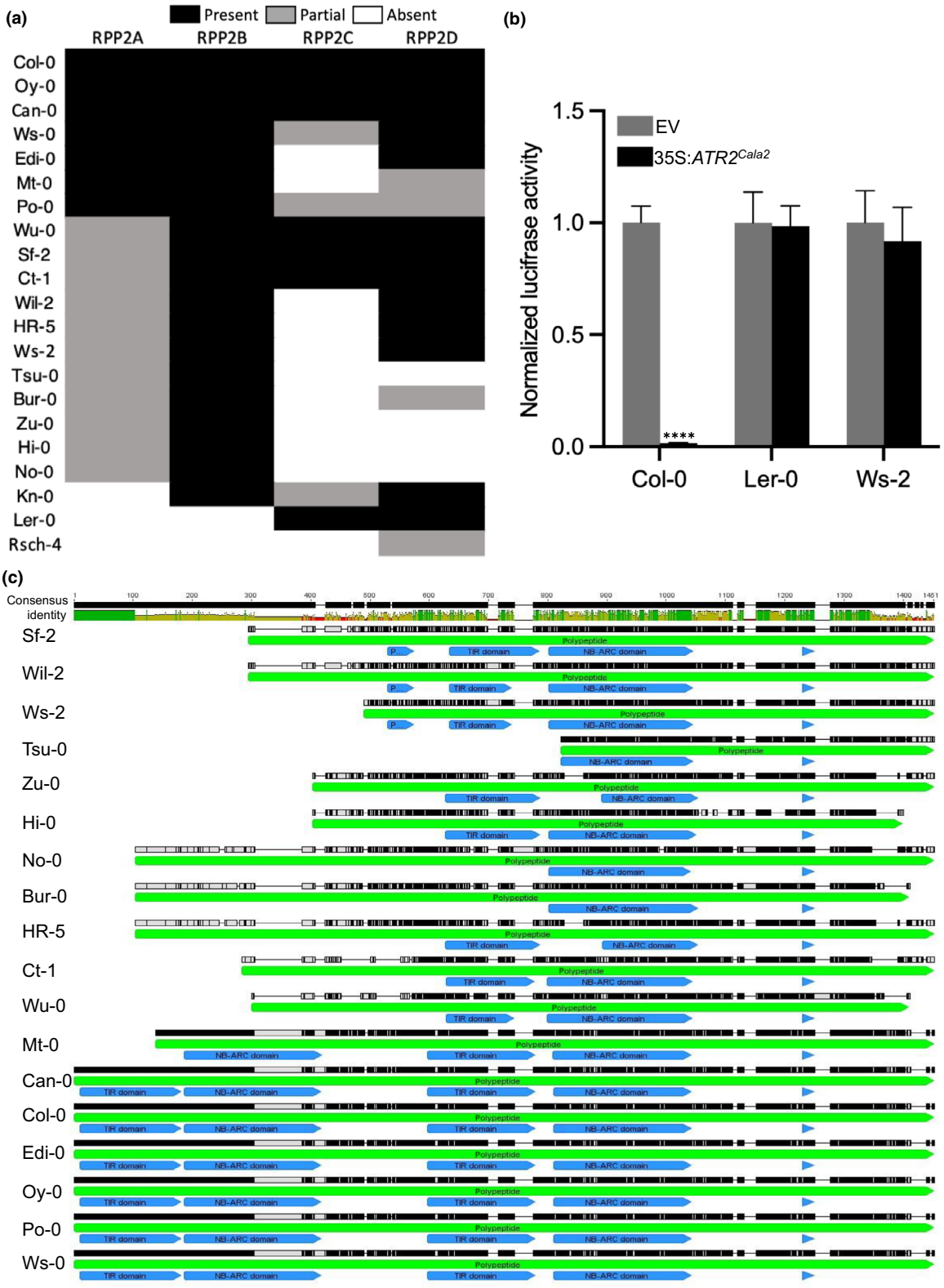

Fig. 5 Differential $ATR2^{Cala2}$ recognition capacity dependent on RPP2A haplotype. (a) Heatmap diagram for *RPP2* cluster haplotype analyses from 21 Arabidopsis ecotypes. (b) Normalized luciferase activity by biolistic bombardment of $ATR2^{Cala2}$ with luciferase into Col-0, Ler-0 (*RPP2A*, *2B*-lacking) and Ws-2 (partial *RPP2A*). Data are means ± SD from three independent experiments. Asterisk indicates a significant difference as determined by two-way ANOVA with Tukey's test (****, $P < 0.0001$). (c) RPP2A haplotype analyses from 21 Arabidopsis ecotypes.

of accessions lack, or contain partial forms of, *RPP2C* or *RPP2D* (Fig. 5a). Among 64 accessions, while only 17 accessions contain complete *RPP2A* encoding TIR-NB-TIR-NB-LRR (TN-TNL) homologues, the *RPP2B*-encoding TIR-NB-LRR (TNL) is well-conserved in almost all accessions excluding Ler-0, Rsch-4 and Vig-1 (Figs S16, S17a). *RPP2C* is lacking or incomplete in > 40 accessions and the amino acid length of RPP2D is quite diverse (Fig. S16). While RPP2A haplotypes show structural diversity on their first TIR-NB-ARC domains, RPP2B, RPP2C and RPP2D are more conserved in different *Arabidopsis* accessions (Fig. S17).

To monitor ATR2^{Cala2} recognition capacity, luciferase eclipse assay bombardment was conducted with Col-0 (complete RPP2 cluster), Ler-0 (*RPP2C* and *RPP2D* lacking) and Ws-2 (partial *RPP2A* and *RPP2C* lacking). As expected, ATR2^{Cala2} is recognized in Col-0, while Ler-0 and Ws-2 lack ATR2^{Cala2} recognition capacity, indicating a critical role of *RPP2A* and *RPP2B* for ATR2^{Cala2} recognition (Fig. 5c). Compared with other *RPP2* genes, *RPP2A* was present in diverse forms. As shown in Fig. 5 (c), diverse accessions including Ws-2 lost the first N-terminal TIR-NB-ARC domain. The TIR-NB-ARC defect in Ws-2 abolishes ATR2^{Cala2} recognition.

Discussion

Downy mildews such as *B. lactucae* on lettuce (Parra *et al.*, 2021), *P. viticola* on grapevines (Li *et al.*, 2015), *P. cubensis* on cucumber (Zhang *et al.*, 2019) and *H. brassicae* on brassicas (Liu *et al.*, 2021) are destructive obligate oomycete phytopathogens on fruit and vegetable crops (Thines & Kamoun, 2010; Tör *et al.*, 2023). Genetic variation for downy mildew resistance has also been studied in *Brassica* species such as *B. napus*, broccoli, non-heading Chinese cabbage and Chinese cabbage (Chen *et al.*, 2008; Xiao *et al.*, 2016). The 27 known *Dm* genes in lettuce are located in gene clusters that encode NLRs (Parra *et al.*, 2021). A better understanding of resistance mechanisms to downy mildew is highly desirable. *Arabidopsis* NLR-encoding *RPP* genes confer recognition of specific downy mildew races and different RPP proteins specifically recognize their cognate downy mildew RxLR effectors (Asai *et al.*, 2018).

Most oomycete pathogens deploy secreted effector proteins, with the signature amino acid motif RxLR, which enter plant cells where they promote virulence (Win *et al.*, 2012; Asai *et al.*, 2014; Wood *et al.*, 2020). The function and evolution of RxLR effectors have been investigated since their discovery (Anderson *et al.*, 2015). Comparative genomics indicates that *RxLR* genes play a major role in virulence for downy mildews and *Phytophthora* species. Although progress has been made, there is still much to learn about the mechanisms of downy mildew virulence and host resistance. Most *P. infestans* and *Hpa* effectors carry an RxLR motif.

We positionally identified *ATR2^{Cala2}* that encodes a non-canonical RxLR-like protein recognized by RPP2A and RPP2B. *ATR2^{Cala2}* encodes an RxLR-like protein with an N-terminal signal peptide, and dEER and C-terminal Y and WY modules. The *ATR2* alleles in other *Hpa* strains are identical to the *ATR2^{Emoy2}* allele and lack GHVR, dEER and WY motifs due to a frame shift resulting from a single nucleotide deletion. In the absence of recognition by *RPP2A* and *RPP2B*, *ATR2^{Cala2}* expression enhances pathogen susceptibility *in planta*. Furthermore, the head-to-head *RPP2C* and *RPP2D* genes, which are adjacent to *RPP2A* and *RPP2B*, also contribute to full resistance to *Hpa*-Cala2. ATR5 was the first example of a non-canonical RxLR effector lacking the canonical RxLR motif but with an N-terminal signal peptide and a canonical EER motif (Bailey *et al.*, 2011). At the expected RxLR position, ATR5 carries Gly-Arg-Val-Arg (GRVR) instead of RxLR. ATR2^{Cala2} at this position carries Gly-His-Val-Arg (GHVR) followed by a dEER motif. ATR5 contains two WY motifs and one LWY motif at its C terminus (Fig. S18a). The Y–WY domain of ATR2^{Cala2} resembles the LWY of ATR5 based on Alphafold2 structural prediction (Fig. S18b). In the *Hpa* genome, > 150 genes encode for potentially secreted proteins such as ATR2^{Cala2} that carry motifs such as signal peptide and EER but lack the RxLR motif (Asai *et al.*, 2014). This also been seen in other oomycetes such as *Pseudoperonospora* and *Bremia* (Purayannur *et al.*, 2020; Wood *et al.*, 2020; Nur *et al.*, 2023). We conclude that although the RxLR motif is often found in oomycete effectors, in *Hpa* as in other oomycetes, some divergence is permitted for effector translocation. Therefore, additional *Hpa* effectors may exist that have not yet been predicted.

RPP2 was the first genetically defined *R*-gene locus shown to carry two NLR-encoding genes, both of which are required for function (Sinapidou *et al.*, 2004). The corresponding recognized effector from *Hpa* enables investigations into how the *RPP2*-encoded immune receptor complex functions. Recognized effectors are also valuable tools for investigating plant–microbe interactions, since their host targets correspond to important plant defence components. Most *R*-gene pair-encoding NLR proteins, such as *Arabidopsis* RRS1-RPS4 that recognize bacterial effectors AvrRps4 and PopP2, and rice RGA4-RGA5 recognizing rice blast effectors AVR1-CO39 and AVR-Pia, are encoded by divergently transcribed genes (Césari *et al.*, 2013; Ma *et al.*, 2018), in contrast to *RPP2A* and *RPP2B* (Fig. S9a). Sensor NLRs are dependent on executor (or helper) NLRs for downstream immune signalling (Feehan *et al.*, 2020). RRS1 functions as a sensor that reveals effectors that target WRKY domain transcription factors, while RPS4 is an executor (Ma *et al.*, 2018). Uniquely, RPP2A contains two TIR-NB-ARC domains followed by LRR, and an ALOG domain that is specific and conserved to land plants and has DNA-binding activity (Yoshida *et al.*, 2009; Naramoto *et al.*, 2020; Beretta *et al.*, 2023) between the two TIR-NB-ARC domains (Fig. S9). Comparative analyses of RPP2A in diverse *Arabidopsis* accessions show that the main variation in the RPP2A haplotype is the presence or absence of one N-terminal TIR-NB-ARC (Figs 5c, S16). RPP2B is a typical TIR-NLR resembling the executor NLR, RPS4. Compared with RPP2A, RPP2B is relatively well-conserved in different *Arabidopsis* accessions (Figs S16, S17a). Conceivably, RPP2A functions as a sensor for ATR2^{Cala2} and RPP2B functions as a signal executor. TIR domains of plant NLRs are known to have nicotinamide adenine dinucleotide hydrolase (NADase) activity, which requires a catalytic glutamate (E), that activates defence (Wan

et al., 2019). The C-JID domains of *Arabidopsis* RPP1 and *N. benthamiana* ROQ1 (recognition of XopQ1) are required for pathogen effector recognition. ATR1 binds to the C-JID and the LRRs of RPP1 leading to assembly of tetramers with NADase activity (Ma *et al.*, 2020). The LRR and C-JID of ROQ1 directly interact with *Xanthomonas* effector (XopQ), allowing the NB-ARC domain to transition to an ATP-bound state. Complex assembly results in TIR proximity that opens the NADase active site (Martin *et al.*, 2020). The first TIR on RPP2A has the catalytic E residue, whereas the second TIR on RPP2A lacks the conserved E residue (Table S4). The TIR of RPP2B has the conserved E residue and a C-JID (Table S4), consistent with a role as executor. Still, the domains of RPP2A and/or RPP2B that interact with ATR2^{Cala2} remain to be elucidated.

We also revealed the requirement for two additional *TIR-NB-LRR* genes, *RPP2C* and *RPP2D*, adjacent to *RPP2A* and *RPP2B* and showed all four NLR proteins are required for full resistance against *Hpa*-Cala2. A paired head-to-head *R*-gene structure is often found in plant-paired NLRs (Narusaka *et al.*, 2009; Césari *et al.*, 2014; Saucet *et al.*, 2021). *RPP2C* and *RPP2D* form a head-to-head orientation similar to *RRS1-RPS4* (Narusaka *et al.*, 2009; Ma *et al.*, 2018; Guo *et al.*, 2020). The C-terminal post-LRR domain of RPS4 is homologous with C-JID suggesting that it recognizes conformational changes in RRS1 upon effector recognition (Saucet *et al.*, 2021). The RPP2C post-LRR domain is homologous to that of RRS1 but RPP2C contains a TIR domain on its C-terminal end instead of WRKY. RPP2D contains a C-JID on its C terminus homologous to that of RPS4 and RPP1 (Fig. S9; Table S4). Many *Arabidopsis* accessions lack or have incomplete RPP2C but RPP2D is relatively conserved among different accessions (Fig. S16). Even though *RPP2C* and *RPP2D* are quantitatively required for full resistance against *Hpa*-Cala2, how this pair contributes to ATR2^{Cala2} recognition remains unclear. Conceivably, their contribution could either be additive, or by potentiating RPP2A/B-dependent recognition. We speculate that since both RPP2A and RPP2C carry integrated TIR domains, which do not contain a catalytic E residue, ATR2^{Cala2} might function by interacting with and somehow suppressing functions of host TIR domain-containing proteins. RPP4, a TIR-NLR, can mediate HR upon detection of *Hpa* RxLR effector AvrRPP4 (Asai *et al.*, 2018). ATR2^{Cala2} transient expression could not suppress RPP4-mediated HR (Fig. S19). Interestingly, the TIR on RPP2C C-terminal end lacks the catalytic E residue for NADase activity, while the first TIR on RPP2C has the E residue, and RPP2D also has the E residue on its TIR (Table S4). We hypothesize that the second TIR on RPP2A might function to detect ATR2^{Cala2} leading to conformational change via RPP2B interaction with ATR2^{Cala2}. This could result in RPP2A/B resistosome activation enabling signal transduction through activated NADase function of the first TIR on RPP2A and RPP2B TIR. If the TIR in RPP2A lacking catalytic E functions as an effector decoy, the C-terminal TIR on RPP2C might also act as an integrated decoy to detect ATR2^{Cala2}. However, thus far we were unable to detect direct or indirect interaction between ATR2^{Cala2} and each RPP2 protein (Fig. S14). Even though *RPP2C* expression was abundantly detected by reverse transcription polymerase chain reaction (Fig. S15), no signal was detected for C-terminal epitope tagged RPP2C by Western blot (Fig. S14). Searching for the actual splicing pattern of 3′ of *RPP2C* and determining its encoding amino acid sequence is required to investigate the mechanisms of an NLR complex involving four TNL proteins. Further research is needed to define the effector recognition mechanisms for these atypical NLR protein pairs.

Acknowledgements

Financial support from the Gatsby Charitable Foundation (http://www.gatsby.org.uk/), and from BBSRC grants BB/K009176/1 and BB/M003809/1 to JDGJ, is gratefully acknowledged. This work is also supported in part by the grant 09 963/A from the Leverhulme Trust to MT. We thank Matthew Smoker and Jodie Taylor for their help with *Arabidopsis* transformation. The authors would like to thank Dr Kenichi Tsuda for providing luciferase assay kit for DSK.

Competing interests

None declared.

Author contributions

DSK, MT and JDGJ conceptualized and designed the research. DSK, AW-T, VC and OJF conducted all experiments. DSK and MT performed the data analysis. VC and MT gave critical intellectual input and provided materials for this work. YL and WM carried out structural prediction and analyses of *Hpa* effectors. H-KA carried out protein-complex analyses. DSK, MT and JDGJ wrote the manuscript with input from all co-authors.

ORCID

Hee-Kyung Ahn https://orcid.org/0000-0002-8884-0156
Volkan Cevik https://orcid.org/0000-0002-3545-3179
Oliver J. Furzer https://orcid.org/0000-0002-3536-9970
Jonathan D. G. Jones https://orcid.org/0000-0002-4953-261X
Dae Sung Kim https://orcid.org/0000-0002-4579-2094
Yufei Li https://orcid.org/0000-0003-0245-3807
Wenbo Ma https://orcid.org/0000-0001-5569-639X
Mahmut Tör https://orcid.org/0000-0002-4416-5048

Data availability

All the sequence data used in this study can be found in NCBI (see the Materials and Methods section; https://www.ncbi.nlm.nih.gov/sra/SRX13788375; https://www.ncbi.nlm.nih.gov/sra/SRX13788374; https://www.ncbi.nlm.nih.gov/nuccore/ON994189.1/; https://www.ncbi.nlm.nih.gov/nuccore/ON994190.1/; https://www.ncbi.nlm.nih.gov/bioproject/PRJNA955397/).

References

Allen RL, Bittner-Eddy PD, Grenville-Briggs LJ, Meitz JC, Rehmany AP, Rose LE, Beynon JL. 2004. Host-parasite coevolutionary conflict between *Arabidopsis* and downy mildew. *Science* **306**: 1957–1960.

Anderson RG, Deb D, Fedkenheuer K, McDowell JM. 2015. Recent progress in RXLR effector research. *Molecular Plant–Microbe Interactions* **28**: 1063–1072.

Asai S, Furzer OJ, Cevik V, Kim DS, Ishaque N, Goritschnig S, Staskawicz BJ, Shirasu K, Jones JDG. 2018. A downy mildew effector evades recognition by polymorphism of expression and subcellular localization. *Nature Communications* **9**: 5192.

Asai S, Rallapalli G, Piquerez SJM, Caillaud MC, Furzer OJ, Ishaque N, Wirthmueller L, Fabro G, Shirasu K, Jones JDG. 2014. Expression profiling during Arabidopsis/downy mildew interaction reveals a highly-expressed effector that attenuates responses to salicylic acid. *PLoS Pathogens* **10**: e1004443.

Bailey K, Cevik V, Holton N, Byrne-Richardson J, Sohn KH, Coates M, Woods-Tör A, Aksoy HM, Hughes L, Baxter L *et al.* 2011. Molecular cloning of ATR5^{Emoy2} from *Hyaloperonospora arabidopsidis*, an avirulence determinant that triggers RPP5-mediated defense in *Arabidopsis*. *Molecular Plant–Microbe Interactions* **24**: 827–838.

Baxter L, Tripathy S, Ishaque N, Boot N, Cabral A, Kemen E, Thines M, Ah-Fong A, Anderson R, Badejoko W *et al.* 2010. Signatures of adaptation to the obligate biotrophy in the *Hyaloperonospora arabidopsidis* genome. *Science* **330**: 1549–1551.

Beretta VM, Franchini E, Ud Din I, Lacchini E, Van den Broeck L, Sozzani R, Orozco-Arroyo G, Caporali E, Adam H, Jouannic S *et al.* 2023. The ALOG family members OsG1L1 and OsG1L2 regulate inflorescence branching in rice. *The Plant Journal* **115**: 351–368.

Bernoux M, Ve T, Willams S, Warren C, Hatters D, Valkov E, Zhang X, Ellis JG, Kobe B, Dodds PN. 2011. Structural and functional analysis of a plant resistance protein TIR domain reveals interfaces for self-association, signaling, and autoregulation. *Cell Host & Microbe* **9**: 200–211.

van der Biezen EA, Freddie CT, Kahn K, Parker JE, Jones JDG. 2002. *Arabidopsis RPP4* is a member of the *RPP5* multigene family of TIR-NB-LRR genes and confers downy mildew resistance through multiple signalling components. *The Plant Journal* **29**: 439–451.

Birch PRJ, Rehmany AP, Pritchard L, Kamoun S, Beynon JL. 2006. Trafficking arms: oomycete effectors enter host plant cells. *Trends in Microbiology* **14**: 8–11.

Bomblies K, Lempe J, Warthmann N, Lanz C, Dangl JL, Weigel D. 2007. Autoimmune response as a mechanism for a Dobzhansky-Muller-type incompatibility syndrome in plants. *PLoS Biology* **5**: e236.

Botella MA, Parker JE, Frost LN, Bittner-Eddy PD, Beynon JL, Daniels MJ, Holub EB, Jones JDG. 1998. Three genes of the Arabidopsis *RPP1* complex resistance locus recognize distinct *Peronospora parasitica* avirulence determinants. *Plant Cell* **10**: 1847–1860.

Boutrot F, Zipfel C. 2017. Function, discovery, and exploitation of plant pattern recognition receptors for broad-spectrum disease resistance. *Annual Review of Phytopathology* **55**: 257–286.

Césari S, Kanzaki H, Fujiwara T, Bernoux M, Chalvon V, Kawano Y, Shimamoto K, Dodds P, Terauchi R, Kroj T. 2014. The NB-LRR proteins RGA4 and RGA5 interact functionally and physically to confer disease resistance. *EMBO Journal* **33**: 1941–1959.

Césari S, Thilliez G, Ribot C, Chalvon V, Michel C, Jauneau A, Rivas S, Alaux L, Kanzaki H, Okuyama Y *et al.* 2013. The rice resistance protein pair RGA4/RGA5 recognizes the *Magnaporthe oryzae* effectors AVR-Pia and AVR1-CO39 by direct binding. *Plant Cell* **25**: 1463–1481.

Chen XF, Hou XL, Zhang JY, Zheng JQ. 2008. Molecular characterization of two important antifungal proteins isolated by downy mildew infection in non-heading Chinese cabbage. *Molecular Biology Reports* **35**: 621–629.

Chisholm ST, Coaker G, Day B, Staskawicz BJ. 2006. Host–microbe interactions: shaping the evolution of the plant immune response. *Cell* **124**: 803–814.

Clough SJ, Bent AF. 1998. Floral dip: a simplified method for *Agrobacterium*-mediated transformation of *Arabidopsis thaliana*. *The Plant Journal* **16**: 735–743.

Coates ME, Beynon JL. 2010. *Hyaloperonospora arabidopsidis* as a pathogen model. *Annual Review of Phytopathology* **48**: 329–345.

Dangl JL, Horvath DM, Staskawicz BJ. 2013. Pivoting the plant immune system from dissection to deployment. *Science* **341**: 746–751.

Dodds PN, Rathjen JP. 2010. Plant immunity: towards an integrated view of plant–pathogen interactions. *Nature Reviews Genetics* **11**: 539–548.

Eitas TK, Dangl JL. 2010. NB-LRR proteins: pairs, pieces, perceptions, partners, and pathways. *Current Opinion in Plant Biology* **13**: 472–477.

Ellis JG, Dodds PN, Lawrence GJ. 2007. Flax rust resistance gene specificity is based on direct resistance-avirulence protein interactions. *Annual Review of Phytopathology* **45**: 289–306.

Feehan JM, Castel B, Bentham AR, Jones JDG. 2020. Plant NLRs get by with a little help from their friends. *Current Opinion in Plant Biology* **56**: 99–108.

Feng F, Zhou JM. 2012. Plant-bacterial pathogen interactions mediated by type III effectors. *Current Opinion in Plant Biology* **15**: 469–476.

Geu-Flores F, Nour-Eldin HH, Nielsen MT, Halkier BA. 2007. USER fusion: a rapid and efficient method for simultaneous fusion and cloning of multiple PCR products. *Nucleic Acids Research* **35**: e55.

Goritschnig S, Krasileva KV, Dahlbeck D, Staskawicz BJ. 2012. Computational prediction and molecular characterization of an oomycete effector and the cognate *Arabidopsis* resistance gene. *PLoS Genetics* **8**: e1002502.

Guo H, Ahn HK, Sklenar J, Huang J, Ma Y, Ding P, Menke FLH, Jones JDG. 2020. Phosphorylation-regulated activation of the *Arabidopsis* RRS1-R/RPS4 immune receptor complex reveals two distinct effector recognition mechanisms. *Cell Host & Microbe* **27**: 769–781.

He J, Ye W, Choi DS, Wu B, Zhai Y, Guo B, Duan S, Wang Y, Gan J, Ma W *et al.* 2019. Structural analysis of *Phytophthora* suppressor of RNA silencing 2 (PSR2) reveals a conserved modular fold contributing to virulence. *Proceedings of the National Academy of Sciences, USA* **116**: 8054–8059.

Høie MH, Kiehl EN, Petersen B, Nielsen M, Winther O, Nielsen H, Hallgren J, Marcatili P. 2022. NetSurfP-3.0: accurate and fast prediction of protein structural features by protein language models and deep learning. *Nucleic Acids Research* **50**: W510–W515.

Holub EB. 2008. Natural history of *Arabidopsis thaliana* and oomycete symbioses. *European Journal of Plant Pathology* **122**: 91–109.

Holub EB, Beynon JL, Crute IR. 1994. Phenotypic and genotypic characterisation of interactions between isolates of *Peronospora parasitica* and accessions of *Arabidopsis thaliana*. *Molecular Plant–Microbe Interactions* **7**: 223–239.

Hou Y, Zhai Y, Feng L, Karimi HZ, Rutter BD, Zeng L, Choi DS, Zhang B, Gu W, Chen X *et al.* 2019. A *Phytophthora* effector suppresses trans-kingdom RNAi to promote disease susceptibility. *Cell Host & Microbe* **25**: 153–165.

Jones DA, Takemoto D. 2004. Plant innate immunity – direct and indirect recognition of general and specific pathogen-associated molecules. *Current Opinion in Immunology* **16**: 48–62.

Jones JDG, Dangl JL. 2006. The plant immune system. *Nature* **444**: 323–329.

Jones JDG, Vance RE, Dangl JL. 2016. Intracellular innate immune surveillance devices in plants and animals. *Science* **354**: aaf6395.

Jumper J, Evans R, Pritzel A, Green T, Figurnov M, Ronneberger O, Tunyasuvunakool K, Bates R, Žídek A, Potapenko A *et al.* 2021. Highly accurate protein structure prediction with AlphaFold. *Nature* **596**: 583–589.

Kim DS, Kim NH, Hwang BK. 2015. Glycine-rich RNA-binding protein1 interacts with receptor-like cytoplasmic protein kinase1 and suppresses cell death and defense responses in pepper (*Capsicum annuum*). *New Phytologist* **205**: 786–800.

Krasileva KV, Dahlbeck D, Staskawicz BJ. 2010. Activation of an *Arabidopsis* resistance protein is specified by the *in planta* association of its leucine-rich repeat domain with the cognate oomycete effector. *Plant Cell* **22**: 2444–2458.

Li H, Yu SC, Zhang FL, Yu YJ, Zhao XY, Zhang DS, Zhao X. 2011. Development of molecular markers linked to the resistant QTL for downy mildew in *Brassica Rapa* L. ssp. *pekinensis*. *Hereditas* **33**: 1271–1278.

Li X, Wu J, Yin L, Zhang YL, Qu JJ, Lu J. 2015. Comparative transcriptome analysis reveals defense-related genes and pathways against downy mildew in *Vitis amurensis* grapevine. *Plant Physiology and Biochemistry* **95**: 1–14.

Lin X, Jia Y, Heal R, Prokchorchik M, Sindalovskaya M, Olave-Achury A, Makechemu M, Fairhead S, Noureen A, Heo J *et al.* 2023. *Solanum americanum* genome-assisted discovery of immune receptors that detect potato late blight pathogen effectors. *Nature Genetics* **55**: 1579–1588.

Lin X, Olave-Achury A, Heal R, Pais M, Witek K, Ahn HK, Zhao H, Bhanvadis A, Karki HS, Song T *et al.* 2022. A potato late blight resistance gene protects against multiple *Phytophthora* species by recognizing a broadly conserved RXLR-WY effector. *Molecular Plant* **15**: 1457–1469.

Liu Y, Li D, Yang N, Zhu X, Han K, Gu R, Bai J, Wang A, Zhang Y. 2021. Genome-side identification and analysis of CC-NBS-LRR family in response to downy mildew and black rot in Chinese cabbage. *International Journal of Molecular Sciences* **22**: 4266.

Ma S, Lapin D, Liu L, Sun Y, Song W, Zhang X, Logemann E, Yu D, Wang J, Jirschitzka J *et al.* 2020. Direct pathogen-induced assembly of an NLR immune receptor complex to form a holoenzyme. *Science* **370**: eabe3069.

Ma Y, Guo H, Hu L, Martinez PP, Moschou PN, Cevik V, Ding P, Duxbury Z, Sarris PF, Jones JDG. 2018. Distinct modes of derepression of an Arabidopsis immune receptor complex by two different bacterial effectors. *Proceedings of the National Academy of Sciences, USA* **115**: 10218–10227.

Martin R, Qi T, Zhang H, Liu F, King M, Toth C, Staskawicz BJ. 2020. Structure of the activated Roq1 resistosome directly recognizing the pathogen effector XopQ. *Science* **370**: eabd9993.

Meyers BC, Kozik A, Kuang H, Michelmore RW. 2003. Genome-wide analysis of NBS-LRR-encoding genes in Arabidopsis. *Plant Cell* **15**: 809–834.

Monaghan J, Zipfel C. 2012. Plant pattern recognition receptor complexes at the plasma membrane. *Current Opinion in Plant Biology* **15**: 349–357.

Naramoto S, Hata Y, Kyozuka J. 2020. The origin and evolution of the ALOG proteins, members of a plant-specific transcription factor family, in land plants. *Journal of Plant Research* **133**: 323–329.

Narusaka M, Shirasu K, Noutoshi Y, Kubo Y, Shiraishi T, Iwabuchi M, Narusaka Y. 2009. RRS1 and RPS4 provide a dual resistance-gene system against fungal and bacterial pathogens. *The Plant Journal* **60**: 218–226.

Nur MJ, Wood KJ, Michelmore RW. 2023. EffectorO: motif-independent prediction of effectors in oomycete genomes using machine learning and lineage-specificity. *Molecular Plant–Microbe Interactions* **36**: 397–410.

Nürnberger T, Brunner F, Kemmerling B, Piater L. 2004. Innate immunity in plants and animals: striking similarities and obvious differences. *Immunological Reviews* **198**: 249–266.

Oliver RP, Ipcho SV. 2004. Arabidopsis pathology breathes new life into the necrothrphs-vs.-biotrophs classification of fungal pathogens. *Molecular Plant Pathology* **5**: 347–352.

Parra L, Nortman K, Sah A, Truco MJ, Ochoa O, Michelmore R. 2021. Identification and mapping of new genes for resistance to downy mildew in lettuce. *Theoretical and Applied Genetics* **134**: 519–528.

Punta M, Coggill PC, Eberhardt RY, Mistry J, Tate J, Boursnell C, Pang N, Forslund K, Ceric G, Clements J *et al.* 2012. The Pfam protein families database. *Nucleic Acids Research* **40**: D290–D301.

Purayannur S, Cano LM, Bowman MJ, Childs KL, Gent DH, Quesada-Ocampo LM. 2020. The effector repertoire of the hop downy mildew pathogen *Pseudoperonospora humuli*. *Frontiers in Genetics* **11**: 910.

Redkar A, Cevik V, Bailey K, Zhao H, Kim DS, Zou Z, Furzer OJ, Fairhead S, Borhan MH, Holub EB *et al.* 2023. The Arabidopsis WRR4A and WRR4B paralogous NLR proteins both confer recognition of multiple *Albugo candida* effectors. *New Phytologist* **237**: 532–547.

Rehmany AP, Gordon A, Rose LE, Allen RL, Armstrong MR, Whisson SC, Kamoun S, Tyler BM, Birch PR, Beynon JL. 2005. Differential recognition of highly divergent downy mildew avirulence gene alleles by *RPP1* resistance from two Arabidopsis lines. *Plant Cell* **17**: 1839–1850.

Sánchez-Martín J, Keller B. 2021. NLR immune receptors and diverse types of non-NLR proteins control race-specific resistance in *Triticeae*. *Current Opinion in Plant Biology* **62**: 102053.

Sarris PF, Duxbury Z, Huh SU, Ma Y, Segonzac C, Sklenar J, Derbyshire P, Cevik V, Rallapalli G, Saucet SB *et al.* 2015. A plant immune receptor detects pathogen effectors that target WRKY transcription factors. *Cell* **161**: 1089–1100.

Saucet SB, Esmenjaud D, Van Ghelder C. 2021. Integrity of the post-LRR domain is required for TIR-NB-LRR function. *Molecular Plant–Microbe Interactions* **34**: 286–296.

Sinapidou E, Williams K, Nott L, Bahkt S, Tör M, Crute I, Bittner-Eddy P, Beynon J. 2004. Two TIR:NB:LRR genes are required to specify resistance to *Peronospora parasitica* isolate Cala2 in *Arabidopsis*. *The Plant Journal* **38**: 898–909.

Slusarenko AJ, Schlaich NL. 2003. Downy mildew of *Arabidopsis thaliana* caused by *Hyaloperonospora parasitica* (formerly *Peronospora parasitica*). *Molecular Plant Pathology* **4**: 159–170.

Sohn KH, Lei R, Nemri A, Jones JDG. 2007. The downy mildew effector proteins ATR1 and ATR13 promote disease susceptibility in *Arabidopsis thaliana*. *Plant Cell* **19**: 4077–4090.

Spoel SH, Dong X. 2012. How do plants achieve immunity? Defence without specialized immune cells. *Nature Reviews Immunology* **12**: 89–100.

Thines M, Kamoun S. 2010. Oomycete–plant coevolution: recent advances and future prospects. *Current Opinion in Plant Biology* **13**: 427–433.

Tör M, Wood T, Webb A, Göl D, McDowell JM. 2023. Recent developments in plant-downy mildew interactions. *Seminars in Cell and Developmental Biology* **148-149**: 42–50.

Van de Weyer AL, Monteiro F, Furzer OJ, Nishimura MT, Cevik V, Witek K, Jones JDG, Dangl JL, Weigel D, Bemm F. 2019. A species-wide inventory of NLR genes and alleles in *Arabidopsis thaliana*. *Cell* **178**: 1260–1272.

Varadi V, Anyango S, Deshpande M, Nair S, Natassia C, Yordanova G, Yuan D, Stroe O, Wood G, Laydon A *et al.* 2021. AlphaFold Protein Structure Database: massively expanding the structural coverage of protein-sequence space with high-accuracy models. *Nucleic Acids Research* **50**: D439–D444.

Vleeshouwers VGAA, Raffaele S, Vossen JH, Champouret N, Oliva R, Segretin ME, Rietman H, Cano LM, Lokossou A, Kessel G *et al.* 2011. Understanding and exploiting late blight resistance in the age of effectors. *Annual Review of Phytopathology* **49**: 507–531.

Wan L, Essuman K, Anderson RG, Sasaki Y, Monteiro R, Chung EH, Nishimura EO, DiAntonio A, Milbrandt J, Dangl JL *et al.* 2019. TIR domains of plant immune receptors are NAD^+-cleaving enzymes that promote cell death. *Science* **365**: 799–803.

Win J, Krasileva KV, Kamoun S, Shirasu K, Staskawicz BJ, Banfield MJ. 2012. Sequence divergent RXLR effectors share a structural fold conserved across plant pathogenic oomycete species. *PLoS Pathogens* **8**: e1002400.

Win J, Morgan W, Bos J, Krasileva KV, Cano LM, Chaparro-Garcia A, Ammar R, Staskawicz BJ, Kamoun S. 2007. Adaptive evolution has targeted the C-terminal domain of the RXLR effectors of plant pathogenic oomycetes. *Plant Cell* **19**: 2349–2369.

Wood KJ, Nur M, Gil J, Fletcher K, Lakeman K, Gann D, Gothberg A, Khuu T, Kopetzky J, Naqvi S *et al.* 2020. Effector prediction and characterization in the oomycete pathogen *Bremia lactucae* reveal host-recognized WY domain protein that lack the canonical RXLR motif. *PLoS Pathogens* **16**: e1009012.

Woods-Tör A, Studholme DJ, Cevik V, Telli O, Holub EB, Tör M. 2018. A suppressor/avirulence gene combination in *Hyaloperonospora arabidopsidis* determines race specificity in *Arabidopsis thaliana*. *Frontiers in Plant Science* **9**: 265.

Xiao D, Liu ST, Wei YP, Zhou DY, Hou XL, Li Y, Hu CM. 2016. cDNA-AFLP analysis reveals differential gene expression in incompatible interaction between infected non-heading Chinese cabbage and *Hyaloperonospora parasitica*. *Horticulture Research* **3**: 16034.

Xiong A, Ye W, Choi DS, Wong J, Qiao Y, Tao K, Wang Y, Ma W. 2014. Phytophthora suppressor of RNA silencing 2 is a conserved RxLR effector that promotes infection in soybean and *Arabidopsis thaliana*. *Molecular Plant–Microbe Interactions* **27**: 1379–1389.

Yoshida A, Suzaki T, Tanaka W, Hirano HY. 2009. The homeotic gene *long sterile lemma* (*G1*) specifies sterile lemma identity in the rice spikelet. *Proceedings of the National Academy of Sciences, USA* **106**: 20103–20108.

Zhang P, Zhu Y, Luo X, Zhou S. 2019. Comparative proteomic analysis provides insights into the complex responses to *Pseudoperonospora cubensis* infection of cucumber (*Cucumis sativus* L.). *Scientific Reports* **9**: 9433.

Zhou R, Benavente LM, Stepanova AN, Alonso JM. 2011. A recombineering-based gene tagging system for Arabidopsis. *The Plant Journal* **66**: 712–723.

Supporting Information

Additional Supporting Information may be found online in the Supporting Information section at the end of the article.

Fig. S1 Map-based cloning approach for *ATR2*^{Cala2} allele.

Fig. S2 Diagram of a contig in which *ATR2* candidates co-segregate.

Fig. S3 Loci, structure and recognition of *A2C1* and *A2C2*.

Fig. S4 *A2C1* and *A2C2* do not trigger cell death with *RPP2* in *Nicotiana* species.

Fig. S5 Determination of *A2C3*^{Cala2} allele co-segregation on avirulent *Hyaloperonospora arabidopsidis* Cala2-Noks1 F2 population.

Fig. S6 Protein sequence analyses of A2C3^{Cala2}.

Fig. S7 Phylogenetic analysis of post-SP N-terminal sequences of 475 *Hyaloperonospora arabidopsidis* Emoy effectors and A2C3.

Fig. S8 *A2C3* expression after *Hyaloperonospora arabidopsidis* Emoy2 and Cala2 infection.

Fig. S9 Scheme of RPP2 cluster.

Fig. S10 RenSeq-MiSeq from *rpp2a* mutant. Red triangle indicates 25 bp deletion in *RPP2A*.

Fig. S11 Compromised ATR2-mediated resistance in *rpp2* mutants.

Fig. S12 *Hyaloperonospora arabidopsidis* Emoy2 growth on Col-0, individual *rpp2* mutants and Oy-0.

Fig. S13 No auto-activity causing hypersensitive response was observed from an individual or co-expression of *RPP2* paralogs in *Nicotiana benthamiana*.

Fig. S14 ATR2 is not associated with each RPP2 protein.

Fig. S15 Reverse transcription polymerase chain reaction RT-PCR analyses of *RPP2C* expression.

Fig. S16 RPP2 cluster haplotype analyses from pan-NLRome (Van de Weyer *et al.*, 2019).

Fig. S17 Haplotype analyses of RPP2B, RPP2C and RPP2D.

Fig. S18 Comparison of WY domains of ATR2^{Cala2} and ATR5.

Fig. S19 No suppressive activity of ATR2 on RPP4-triggered hypersensitive response.

Methods S1 Protein gel blot, RenSeq and bioinformatics.

Results S1 Genes in the *ATR2* interval encode effector-like proteins.

Table S1 Interaction phenotypes recorded after inoculation of Col-5 with CaNo F_2 isolates.

Table S2 Mapping table of ATR2.

Table S3 Number of SNPs on A2C3 alleles on seven different *Hyaloperonospora arabidopsidis* isolates.

Table S4 Domains on RPP2 proteins and catalytic E residue conservation on each Toll interleukin-1 receptor.

Please note: Wiley is not responsible for the content or functionality of any Supporting Information supplied by the authors. Any queries (other than missing material) should be directed to the *New Phytologist* Central Office.